ResearchGate

See discussions, stats, and author profiles for this publication at: https://www.researchgate.net/publication/311606411

Wetland Landscape Spatio-Temporal Degradation Dynamics Using the New Google Earth Engine Cloud-Based Platform: Opportunities for Non-Specialists in Remote Sensing

Article *in* Transactions of the ASAE. American Society of Agricultural Engineers · October 2016

DOI: 10.13031/trans.59.11608

CITATIONS
55

READS
3,302

4 authors, including:

Alice Alonso
Université Catholique de Louvain - UCLouvain
9 PUBLICATIONS **141** CITATIONS
SEE PROFILE

R. Muñoz-Carpena
University of Florida
290 PUBLICATIONS **9,210** CITATIONS
SEE PROFILE

Carolina Murcia
Pontificia Universidad Javeriana - Cali
59 PUBLICATIONS **5,348** CITATIONS
SEE PROFILE

All content following this page was uploaded by R. Muñoz-Carpena on 10 June 2017.

The user has requested enhancement of the downloaded file.

WETLAND LANDSCAPE SPATIO-TEMPORAL DEGRADATION DYNAMICS USING THE NEW GOOGLE EARTH ENGINE CLOUD-BASED PLATFORM: OPPORTUNITIES FOR NON-SPECIALISTS IN REMOTE SENSING

A. Alonso, R. Muñoz-Carpena, R. E. Kennedy, C. Murcia

ABSTRACT. *The complex nature of coupled human-natural systems often hinders the identification of forces and mechanisms causing observed environmental changes. The analysis of long-term time series can allow better understanding of those interactions and hence inform more adapted restoration and management programs. However, long-term time series of ground-measured vegetation variables are often not readily available due to the tediousness of the work and the financial and time investment required, especially for large-scale wetland systems. Remote sensing can help overcome this issue by providing more than 40 years of Earth cover images, but until recently the processing and analysis of these images was restricted to experts in remote sensing. The new Google Earth Engine (GEE) opens the remote sensing information mine to engineers or scientists without advanced knowledge in the field, including easy access to petabytes of publicly available remote sensing data and their spatial analysis in the cloud. To illustrate its capabilities, we used GEE to generate time series of the normalized difference vegetation index (NDVI) for the human-impacted Tempisque watershed with its severely degraded downstream Palo Verde wetland in northwest Costa Rica. We detail the processing and analysis steps to facilitate replication to any other case study. After defining the boundary of a study area, any user can generate a list and a video of the Landsat and MODIS images available for the area, NDVI maps, and a time series of the NDVI values spatially aggregated over the study area or a set of previously delineated polygons. One of the challenges we address is discriminating between the multitude of image collections available in the GEE catalog for vegetation mapping. We evaluate and compare the results obtained from five selected Landsat and MODIS image collections and identify the collections that give the best quality results for our case study. We conclude that MODIS is more appropriate for this tropical region because of the higher temporal resolution and hence higher probability to record cloud-free images. NDVI time series from Landsat images demonstrate a significant number of missing values. Landsat maps of NDVI suggest that the entire watershed and protected wetland witnessed an overall increase in vegetation greenness and hence cover since 1986, matching the abandonment of cattle ranching and the known degradation of the wetland by cattail invasion. Within-season vegetation variability can be tracked using MODIS images despite their coarser spatial resolution, showing high variability linked to precipitation patterns in this region. This GEE application illustrates new opportunities for biosystems engineers and other scientists to integrate historical vegetation and land cover data into comprehensive datasets to understand human impacts on ecosystems, and provides the guidance to do so.*

Keywords. *Data, Google Earth Engine, Mapping, NDVI, Remote sensing, Time series, Wetland.*

Wetlands provide a variety of services to humanity, yet they are under increasing pressure from human population resource needs (Mitsch and Gosselink, 2007) and climate change, altering the important functions and services they provide. Wetland conservation, management, and restoration involve long-term monitoring that should span beyond the borders of the wetland and incorporate its landscape (Mitsch and Gosselink, 2000). In addition, this monitoring should include retrospective measurements of targeted variables, ideally over sufficient temporal and spatial domains to recognize changes that would require adaptive management interventions and define reference points for restoration. Long-term monitoring programs can require intensive fieldwork and substantial financial and human investment (e.g., van Dam et al., 1998). Ecosystem-level process-based monitoring costs and effort can grow exponentially when conducted at the landscape scale or for sites that are not easily accessible, such as the estimated 1.3 million ha worldwide

Submitted for review in October 2015 as manuscript number NRES 11608; approved for publication by the Natural Resources & Environmental Systems Community of ASABE in March 2016.

The authors are **Alice Alonso, ASABE Member,** Doctoral Student, and **Rafael Muñoz-Carpena, ASABE Fellow,** Professor, Department of Agricultural and Biological Engineering, University of Florida, Gainesville, Florida; **Robert E. Kennedy,** Assistant Professor, College of Earth, Ocean, and Atmospheric Sciences, Oregon State University, Corvallis, Oregon; **Carolina Murcia,** Science Director, Organization for Tropical Studies, Durham, North Carolina. **Corresponding author:** Rafael Muñoz-Carpena, 281 Frazier Rogers Hall, University of Florida, Gainesville, FL 32611-0570; phone: 352-392-1864; e-mail: carpena@ufl.edu.

Vol. 59(5): 1333-1344 © 2016 American Society of Agricultural and Biological Engineers ISSN 2151-0032 DOI 10.13031/trans.59.11608

of wetland systems (Finlayson and Spiers, 1999). Therefore, many of these ecosystems are poorly documented or not documented at all (Finlayson and Spiers, 1999).

Remote sensing provides an alternative to ground-measured data (Lu et al., 2004). For more than four decades, satellites have spanned the globe to record land properties at broad spatio-temporal scales, providing a unique window into the past to observe the status and dynamics of ecosystems. Remote sensing has been increasingly used to describe and track global land cover and ecosystem status and dynamics, and it is one of the major sources for change detection in large-scale coupled human-natural systems (e.g., Cohen and Goward, 2004; Lu et al., 2004; Gottschalk et al., 2005; Boyd and Danson, 2005). In the case of wetland systems, remotely sensed data have also been successfully used to identify and map vegetation (Adam et al., 2009) and to detect and quantify vegetation succession and ecological shifts through space and time (e.g., Jensen et al., 1987; Christensen et al., 1988; Ramsey and Laine, 1997; Kushwaha et al., 2000; Munyati, 2000; Houhoulis and Michener, 2000; Zhao et al., 2009; Chen et al., 2014).

The last decade witnessed an important change in environmental remote sensing, as several image archives became available cost-free and were processed to a form usable by non-specialists, including Landsat (Wulder et al., 2012), Advanced Very High Resolution Radiometer (AVHRR) (Tucker et al., 2005), and Moderate Resolution Imaging Spectroradiometer (MODIS) (Justice and Townshend, 2002). At the same time, computing capabilities reached the point where advanced analysis could be conducted on large image archives. Together, these advances allowed the remote sensing community to develop analyses that use full image archives to richly describe landscape dynamics, allowing detection and tracking of abrupt changes as well as slowly moving trends through space and time (Kennedy et al., 2009; Kennedy et al., 2014).

Despite these major advances, significant barriers remain to adoption of remote sensing in environmental sciences. A standing challenge is reduction of the noise caused by cloud-contaminated scenes, and identification of the appropriate imagery source that best fits the motivating question. Depending on the spacecraft (e.g., Landsat or MODIS), remotely sensed images differ in their spatial, spectral and temporal resolution and in their temporal coverage. Moreover, images from the same spacecraft can be available in various preprocessed states. Tapping into the algorithms and image archives required specialized expertise and software, powerful computing units, and significant time dedication. Many natural resource engineers, scientists, and managers were still dependent on remote sensing specialists to exploit the potential of satellite imagery information.

In 2010, Google revolutionized the field of remote sensing by launching the Google Earth Engine (GEE) platform (Google, 2015). This geoprocessing cloud-based platform centralizes petabytes of publicly available remotely sensed and ancillary data in the cloud. A large amount of images can be imported with one click on the built-in application programming interface (API) for the JavaScript and Python computer languages, featuring a wide range of algorithms to run geospatial analysis remotely on Google's computational infrastructure. The ease of access to preprocessed and georeferenced data, along with the comprehensive and flexible platform and the computational power and speed gained with the parallelization of operations, opens unlimited possibilities for advanced analysis to geoscientists (e.g., Hansen et al., 2013). GEE also offers potential for the democratization of remote sensing analysis for the broader scientific community. Thanks to the fast and straightforward access to a myriad of remotely sensed data, including a large amount of Landsat and MODIS images, and the well documented geospatial analysis playground, anyone with basic knowledge of remote sensing and coding languages can build a customized dataset from the remote sensing information mine. This should spur the integration of remotely sensed information within a comprehensive dataset to explore changing land and water systems and their integrated management.

In this article, we present a case study illustrating the power of GEE for wetland studies. We focus on the internationally recognized Palo Verde wetland in Costa Rica, which is located in the downstream portion of a highly transformed water-subsidized watershed (Jiménez et al., 2001). It has been severely degraded since the invasion of dense cattail in the early 1980s. The observed alterations are likely a consequence of changes in the socio-economic and environmental landscape introduced by a major infrastructure project consisting of an inter-basin water transfer for hydropower generation and irrigation, along with management practices internal to the park (Osland et al., 2011). However, establishment of causal relationships is challenging because of the high number of interplaying factors. As a result, the watershed and the wetland are mostly managed as a collection of isolated pieces, without considering the interconnected nature of the system in which management decisions propagate in cascading effects and feedback loops. By overlooking the new properties that typically emerge from a complex system (Ottino, 2004), such fragmented management can exacerbate degradation and lead to additional unintended and unexpected consequences. Causal relationships governing such complex systems may be detected through the diagnosis of long-term time series of response and candidate explanatory variables (Hornberger and Spear, 1981; Schreiber, 1999; Sugihara et al., 2012; Larson et al., 2014). For our study area, a significant database of socio-economic, climatological, hydrological, and environmental covariates has already been gathered to perform this analysis. However, historical trends and seasonal patterns of vegetation were lacking. Vegetation is a key response variable in the wetland (Dennison et al., 1993; Adam et al., 2009) and an explanatory variable in the upper part of the watershed. Remote sensing represents a possible solution, but limited resources were available for image processing. By eliminating many barriers to vegetation data collection and processing, GEE can prove critical for readily and quickly generating time series of spatially aggregated vegetation index over delineated areas in the basin.

The objective of this study is to guide non-specialists in remote sensing toward the generation of basic, spatially aggregated vegetation index time series using GEE, and provide insight into the many research opportunities opened by this new tool. We use the Tempisque/Palo Verde case study to illustrate

the procedure used to generate time series of vegetation change from a selected set of image collections generated from Landsat and MODIS sensors and available in the GEE cloud. We present the criteria used to discriminate the most appropriate images to generate the final vegetation time series, and discuss their initial implications for the study of human degradation of the protected Palo Verde wetland.

Materials and Methods

Study Area

Situated in the northern Pacific coast of Costa Rica, the 5,670 km^2 Tempisque watershed was subjected to major transformations in the late 1970s with a large-scale hydropower and irrigation project (fig. 1). Water is transferred from the Caribbean hillside at Lake Arenal and piped through three cascading hydroelectrical jumps before being distributed into the Magdalena River and a network of irrigation channels that spreads through the middle of the Tempisque basin to irrigate more than 44,000 ha of agricultural lands (Zuñiga, 1993; Jiménez et al., 2001). The water eventually flows through the lower basin and into the Pacific Ocean at the Gulf of Nicoya. This development project reshaped the hydrological signature of the watershed and profoundly redefined the land management, from extensive to intensive agriculture (Daniels, 2004; Daniel and Cumming, 2008). It also changed the basin dynamics by altering how the different ecosystems interact with each other. Human decisions at multiple points in space and time propagate in a succession of feedback loops and cascading effects, through the transport and transfer of energy, water, and materials among the different parts. While the mechanisms and forces governing those emerging connections and interactions are still largely unknown (Convertino et al., 2016), their manifestations are already visible in the protected wetland of the Palo Verde National Park (PVNP) in the lower basin (Daniel and Cumming, 2008). This seasonally flooded wetland is internationally recognized under the Ramsar Convention for its stunning biodiversity and for being a nesting and feeding sanctuary for thousands of waterfowls. Beginning in the late 1980s, it has experienced a vegetative regime shift from a heterogeneous landscape with open water, low grasses, and floating and low emergent vegetation with some tall emergent patches of cattail to a monotypic stand of cattail (*Typha domingensis*) (McCoy and Rodriguez, 1994; Vaughan et al., 1996; Calvo-Alvarado and Arias 2005, 2006; Castillo-Núñez and Guzmán, 2004; Trama et al., 2009; Osland et al., 2011). Some areas also exhibit a transition to tropical dry forest. This strongly impacts the biodiversity and services provided by the wetland with, among other effects, a large reduction in the bird population, which is attributed to cattail stands so dense that birds cannot land or feed (Trama et al., 2009).

To identify long-term wetland degradation drivers and elucidate the mechanisms, we intend to explore the cause-effect relationships between the vegetation response variables and a set of hypothesized drivers through the use of time-series analysis (e.g., Hassani, 2007; Sugihara et al., 2012; Detto et al., 2012; Campo-Bescós et al., 2013; Huffaker and Canavari, 2015). Data for the hypothesized drivers are time series of meteorological and hydrological variables measured across the watershed (fig. 1) and indicators for socio-economical temporal dynamics. The results from this data-based diagnostic analysis will inform the further construction of a spatially explicit model.

Time series for each covariate were generated for eleven polygons forming the study area: four for the PVNP and seven for the upstream watershed. Although forming a single body, the PVNP wetland has been described by locals as a cluster of six subwetlands. We combined adjacent small subwetlands in twos to define three polygons for the wetland (fig. 2, zones 1 to 3) and a fourth polygon for the dry land in the PVNP (fig. 2, zone 4). The upper watershed was divided

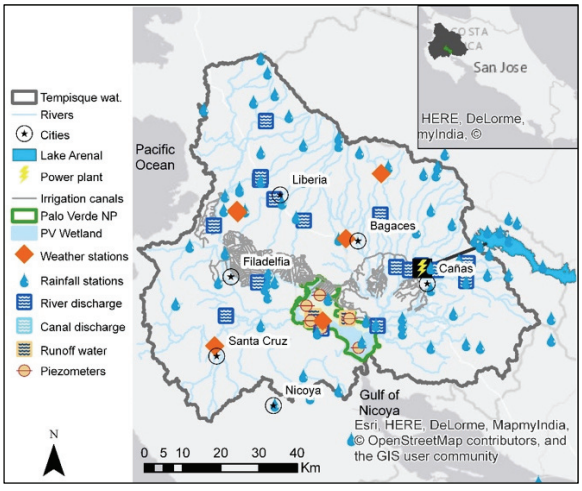

Figure 1. Map of Tempisque watershed including the hydroelectric plant and irrigation network, Palo Verde National Park and its wetland, and the locations of gauge stations for current and past monitoring of hydrological and meteorological variables. The inset localizes the Tempisque watershed and Palo Verde wetland within Costa Rica.

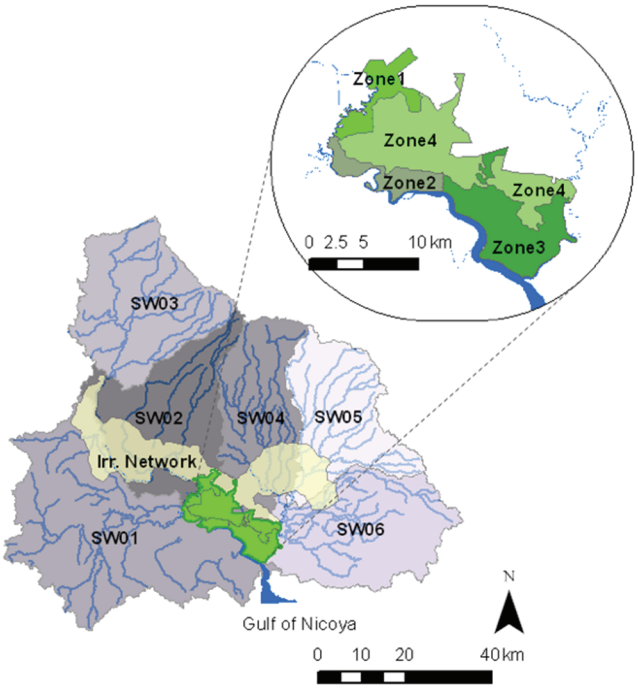

Figure 2. River network and polygon delineation for the Tempisque watershed case study, with a zoom on Palo Verde National Park.

by grouping subwatersheds generated with the Hydrology toolbox in ESRI's ArcMap platform to form six units. An additional polygon corresponding to the current irrigation district surrounded by a 200 m buffer was also considered (fig. 2). All the polygons were delineated and converted into a KMZ file in ArcMap. Their area ranged between 1,924 and 156,413 ha.

Dataset Selection and Calculation of NDVI

Landsat and MODIS Images

The normalized difference vegetation index (NDVI) was used as an indicator for vegetation cover. This index is based on the property that vegetation absorbs electromagnetic radiation in the red region of the spectrum for photosynthesis and scatters solar radiation in the near-infrared spectral region (NIR). It is defined as:

$$\mathrm{NDVI} = \frac{r_{NIR} - r_{red}}{r_{NIR} + r_{red}} \quad (1)$$

where r_{NIR} is the spectral reflectance recorded by an NIR channel, and r_{red} is the spectral reflectance recorded by a red channel. Thus, the NDVI ranges between -1 and 1, with 1 indicating a high density of green leaves, and 0 or negative values indicating no vegetation at all. Soils with high moisture content, such as wetland soils, can influence the electromagnetic signature of vegetation and hence NDVI. However, we considered the index as sufficient to capture the general pattern of vegetation dynamics.

In this study, we compared NDVI generated from Landsat and MODIS images. These two publically available sources are the workhorses of many vegetation dynamics studies (e.g., Cohen and Goward, 2004; Pittman et al., 2010) largely because of their high-quality, well-designed spectral sensitivity and advantageous spatial and temporal resolutions.

The Landsat program, jointly managed by NASA and the U.S. Geological Survey, is the world's longest continuously acquired collection of space-based land remote sensing data. The first satellite (Landsat 1) was launched in 1972 and was followed by a suite of six other sensors, ending with the current Landsat 8 sensor. Each sensor records several spectral bands at different spatial resolutions varying from 15 to 120 m. Landsat satellites perform an entire coverage of the Earth every 16 days. Considering the depth of its archive and its relatively fine spatial resolution, Landsat imagery is especially relevant for fine-scale vegetation mapping. It is increasingly being used to detect subtle ecological processes and changes at fine scales and is particularly promising to detect long-term trends, seasonal patterns, and feedback processes of coupled human and natural systems over smaller and larger scales (Cohen and Goward, 2004; Gottschalk et al., 2005; Boyd and Danson, 2005; Wulder et al., 2012; Kennedy et al., 2014).

The MODIS instruments are mounted on the Terra and Aqua spacecraft, which were launched by NASA in December 1999 and May 2002, respectively, with the objective to generate a long-term dataset of land data (Justice and Townshend, 2002). Both satellites cover the Earth's surface every one to two days with distinct orbits, resulting in different viewing and cloud cover conditions for a specific location. The MODIS instruments record data in 36 spectral bands with a spatial resolution of 250 m to 1 km. MODIS images are particularly suited to map vegetation and land cover at regional to global scales and track changes at fine temporal resolutions.

For this study, we did not use several other publicly and privately owned image sources, including AVHRR, SPOT, IKONOS, and Quickbird (Xie et al., 2008). AVHRR has a spatial resolution too coarse for this study (8 km), and SPOT has not been openly released for Central America yet. Furthermore, they have not been included in the GEE data catalog at the time of this study, although we expect AVHRR images and the open-access portion of SPOT images to be included soon. The higher spatial resolution sources (IKONOS and Quickbird) are rapidly building impressive long-term archives, but currently they do not have the temporal depth needed to understand feedback processes in our system.

Image Sources on GEE for Vegetation Mapping

GEE hosts multiple Landsat and MODIS datasets usable for NDVI mapping. They differ by the craft that recorded the data, the preprocessing status of the images, whether or not a vegetation index has been calculated at the pixel scale for those images, and whether or not they have been aggregated to form composites at a specific temporal resolution (usually 8 days, 16 days, 32 days, annual, 3 years, or 5 years). For many new users, it is challenging to discriminate among these different datasets for appropriate use. We tested the five Landsat and MODIS sets of images and composites (hereafter referred to as collections) with a temporal resolution shorter than one month (table 1). In the case of LAN.G-8dNDVI, we opted for the 8-day composites over the 32-day composites also provided by Google. In the 32-day composites, the NDVI value at each pixel and for each period is the value from the most recent pixel. Alternatively, the 8-day resolution allows selection of the maximal monthly value, which eliminates possible lower NDVI values due to cloud contamination.

The LAN.G-8dNDVI and MODIS collections came by default with an NDVI band generated by the provider. For the LAN.LDEDAPS and LAN.TAO collections, NDVI values were calculated in the GEE API from the NIR and red bands with the built-in *normalizeDifference* function (Google, 2015) and added as a band to each image in the collections.

Spatially aggregated NDVI time series were generated by calculating the median of the NDVI value of each pixel populating a selected area. As a first step, the NDVI values were aggregated over the entire Tempisque watershed for the five selected image collections. The resulting time series were compared to each other, and the collections that gave the most satisfactory results were retained. The criteria for the selection were the length of record, the number of images available and their temporal distribution, the apparent noise, and the pixel size. The final collections were used to generate the NDVI time series for the eleven delineated polygons (fig. 2).

Table 1. Properties of image collections selected for NDVI calculation and mapping in the Tempisque case study.

Image Collection and Corresponding ID in GEE	Description	Start and End Dates	Spatial / Temporal Resolution	Pros (+) and Cons (-)
Landsat TOA (LAN.TOA)				
LANDSAT/LT4_L1T_TOA LANDSAT/LT5_L1T_TOA LANDSAT/LE7_L1T_TOA LANDSAT/LC8_L1T_TOA	L1T orthorectified and calibrated Landsat top-of-atmosphere (TOA) reflectance collections from Landsat 4, 5, 7, and 8 scenes. TOA reflectance is the relative return of radiation leaving the outside of the atmosphere compared to what went in. Any atmospheric effects, such as haze or moisture, are convolved with the signal.	Oct. 1984 to Aug. 2015	30 m / 16 days	+ Landsat 4, 5, 7, and 8 in the GEE data catalog. + Finer spatial resolution. + Longer temporal cover than MODIS. + Metadata, including cloud cover. + Thermal band allowing estimation of cloud cover at pixel scale. - Smaller temporal resolution than MODIS. - Many missing scenes for the area under study. - More variability between images. - NDVI has to be computed by user.
Landsat LEDAPS (LAN.LEDAPS)				
LEDAPS/LT5_L1T_SR LEDAPS/LE7_L1T_SR	LAN.TOA adjusted to Landsat surface reflectance imagery calculated by removing atmospheric effects using the LEDAPS algorithms (Masek et al., 2006).	Oct. 1984 to Aug. 2015	30 m / 16 days	Same as LAN.TOA, unless: + Corrected for atmospheric noise. + Less variability between images. - Only Landsat 5 and 7 are in the GEE data catalog so far. - No thermal band.
Landsat 8 days NDVI (LAN.G-8dNDVI)				
LANDSAT/LT4_L1T_8DAY_NDVI LANDSAT/LT5_L1T_8DAY_NDVI LANDSAT/LE7_L1T_8DAY_NDVI LANDSAT/LC8_L1T_8DAY_NDVI	Composites generated by Google from LAN.TOA scenes. Images include a single band for NDVI. The NDVI value at each pixel and for each period is the value from the most recent pixel.	June 1984 to Aug. 2015	30 m / 8 days	Same as LAN.TOA unless: + NDVI included as a band. - No metadata for cloud cover.
MODIS – U. 16 days VI (MOD.U-16dNDVI)				
MODIS/MOD13Q1 MODIS/MYD13Q1	Generated by USGS-LPDAAC from atmospherically corrected bidirectional surface reflectance and masked for water, clouds, heavy aerosols, and cloud shadows. Images include two NDVI and EVI (enhanced vegetation index) bands. Scenes from the Terra and Aqua sensors are in two distinct collections. The VI in those datasets are multiplied by 10,000 to facilitate storage.	Feb. 2000 to July 2015	250 m / 16 days	+ Finer spatial resolution than MOD.G-16dNDVI. + NDVI included as a band. + Higher temporal resolution than Landsat. + No missing scenes. - Shorter temporal coverage than Landsat. - Coarser spatial resolution than Landsat. - No metadata for cloud cover.
MODIS – G. 16 days VI (MOD.G-16dNDVI)				
MODIS/MCD43A4_NDVI	Generated by Google by calculating the NDVI from the MODIS MCD43A4 composite. Images include a single NDVI band. MCD43A4 is released by USGS-LPDAAC and includes scenes from the Terra and Aqua sensors with reflectance data adjusted using a bidirectional reflectance distribution function (BRDF) to model the values as if they were acquired with a nadir-viewing sensor. BRDF corrects temporal variation caused by view and illumination geometry.	Feb. 2000 to July 2015	500 m / 16 days	Same as MOD.U-16dNDVI unless: + Corrected for BRDF effects. - Coarser spatial resolution.

Implementation in GEE

NDVI time series are aggregated with the GEE playground, a web-based integrated development environment (IDE) that interfaces with underlying image processing libraries through either a Python or JavaScript API (Google, 2015). The libraries contain an extensive and constantly growing data catalog with petabytes of open-access preprocessed and georeferenced images (rasters) and features (vectors) that can readily be imported on the playground to run geospatial analysis. This interface also features many other capabilities (fig. 3). Every user has access to personal and shared scripts when logging into a personal GEE account, and user-generated scripts are accessible for sharing through URL hyperlinks (see the "Supplementary Material" section at the end of this article for the URL of our script for this study). GEE is a developing platform whose access is still limited to a restricted number of developers. However, users from public institutions are likely to be granted full access rights.

GEE was used to implement a sequence of processing steps to construct and examine the NDVI time series in the study area (fig. 4). The same procedure was applied for the five collections evaluated in this study (table 1). The images available for the study area were listed and visualized on

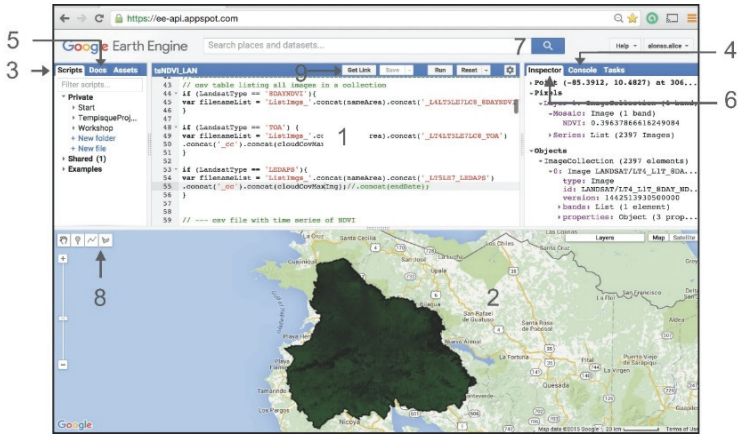

Figure 3. Screenshot of the GEE playground and its main features: (1) code editor, (2) visualization interface, (3) private and personal script manager, (4) console displaying errors and outputs, (5) API reference documentation, (6) map inspector, (7) data catalog search bar, (8) geometry drawing tool, and (9) link for script access and sharing.

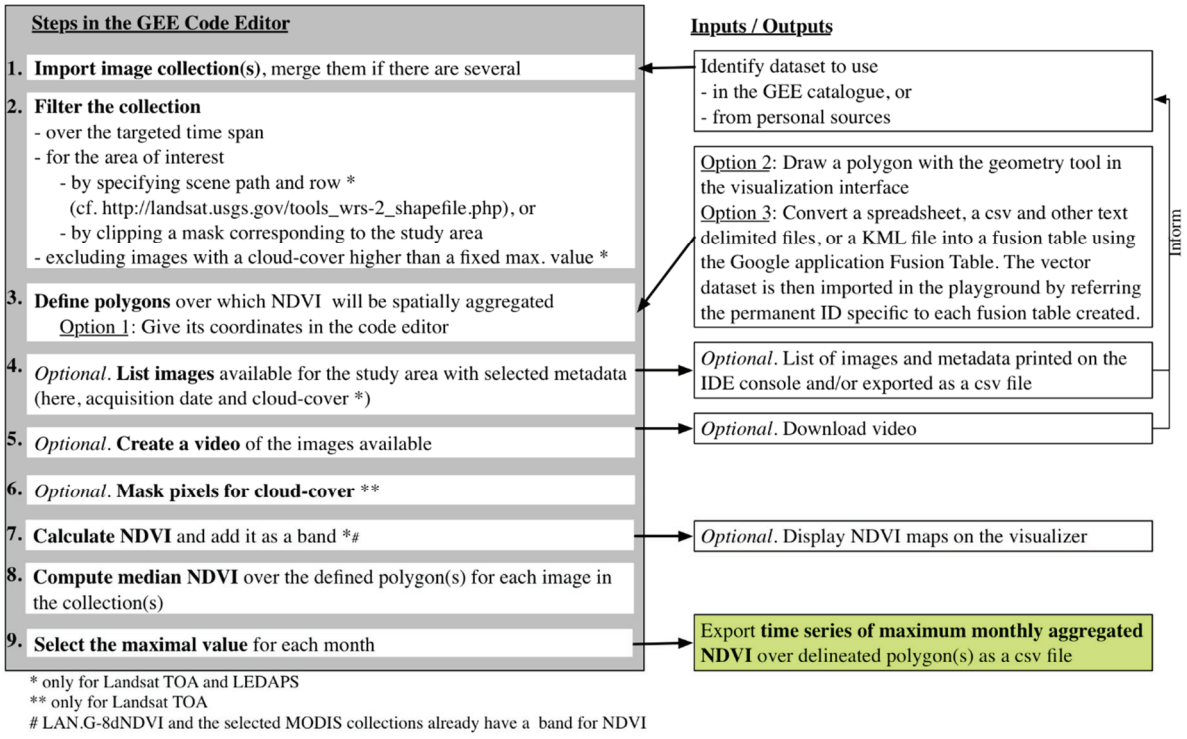

Figure 4. Flowchart of the steps implemented in the GEE API to obtain time series of spatially aggregated NDVI over a user-defined area, along with the inputs and outputs.

GEE and with videos (fig. 4, steps 4 and 5). The noise caused by cloud contamination was reduced using a three-step approach. When ancillary data for a selected collection were available, images with cloud cover greater than 25% were disregarded (fig. 4, step 2). Pixels with cloud cover greater than 15% were masked using the GEE *simpleCloudScore* function (fig. 4, step 6). This was only implemented on LAN.TOA images, the only collection that included the thermal band required by the function. Eventually, each aggregated NDVI time series was converted to monthly resolution by selecting the maximal values in each month as the last step in the process (fig. 4, step 9). We assumed the NDVI variation in each month to be the result of cloud and other atmospheric contamination; hence, selecting the maximal value was an additional step to reduce this source of noise. The monthly time series generated before and after this noise reduction procedure were compared to evaluate the performance of this step.

Results and Discussion

Image Availability for Tempisque Watershed

Images available in each collection for the study area were displayed in videos (see the "Supplementary Material" section) and listed along with their ancillary data in GEE. The videos indicated that many Landsat scenes exhibited significant cloud cover, but the clouds were often located

outside of the study area, in the northeast mountainous region and above the Pacific Ocean. We thus accepted images with as much as 25% cloud cover for further analysis. The total number of images and the number of months with at least one image available in the GEE archive are summarized in table 2. The Landsat collections have a significant number of missing images, with 44%, 49%, and 38% of months without data for the LAN.TOA, LAN.LEDAPS, and LAN.G-8dNDVI collections, respectively. This lack of imagery is partially explained by the high cloud cover characteristic of this tropical region, particularly during the rainy season from May to October (fig. 5a). The number of images available during this season is therefore lower, especially after the dataset was cleared of images with cloud cover greater than 25% (fig. 5b). The exclusion of those images increased the proportion of months without usable images to 65% and 70% for LAN.TOA and LAN.LEDAPS, respectively (table 2). Other factors behind the lack of data might be technical, including periods when non-U.S. downlink stations could not be operated, periods when image collection was de-prioritized over non-U.S. holdings, and failure of the TDRS transmitter onboard the Landsat 5 spacecraft in 1985. At that time, the satellite could only acquire imagery over regions of the world where ground stations were operating. This resulted in massive data gaps in some regions of the globe from 1985 to 1999, when Landsat 7 was launched. The longer data gaps observed until 1996 (figs. 6a to 6c) support this hypothesis. Figures 6a to 6c also clearly show the role of filtering in removing noise from clouds. The three Landsat time series exhibited a seemingly noisy signal when all images were included, while clear successions of decreasing NDVI values appeared annually during the dry season on filtered LAN.TOA and LAN.LEDAPS collections. Because images from LAN.G-8dNDVI had no cloud cover metadata, they could not be readily filtered for cloud cover, and hence the noise remained. This is a flaw of this dataset. Conversely, the MODIS collections hold at least one image per month (table 2) over the period of time during which the Terra and Aqua sensors have been operating. The coherent structure of the maximum monthly time series (figs. 6d and 6e) suggests that there is at least one image a month with minimal cloud contamination. With a temporal resolution of one or two days and passage of the Terra and Aqua satellites at two different moments of the day, the MODIS data have a much higher probability of obtaining at least one cloud-free image per month.

Table 2. Number of images available per collection over the study area. The numbers 100 and 25 for the Landsat collections indicate the cloud cover thresholds (%) under which images were selected. The numbers in parentheses in the second column indicate the number of images per satellite (Landsat 4, 5, 7, and 8; MODIS Terra and Aqua). The number of months without images and the percentage were calculated based on the dates of the first and last available images.

Collection	Total Number of Images (and Number per Satellite)	Number of Months without Images (and Percentage of Total Duration)
LAN.TOA 100	332 (17, 102, 164, 50)	164 (44%)
LAN.TOA 25	184 (00312, 66, 83, 23)	241 (65%)
LAN.LEDAPS 100	263 (101, 162)	180 (49%)
LAN.LEDAPS 25	147 (65, 82)	258 (70%)
LAN.G-8dNDVI	2715 (522, 1305, 772, 116)	143 (38%)
MOD.U-16dNDVI	657 (356, 301)	0 (0%)
MOD.G-16dNDVI	710 (NA)	0 (0%)

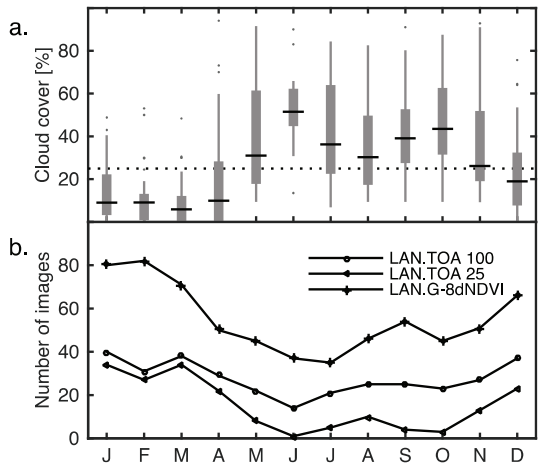

Figure 5. (a) Boxplot of cloud cover percentage per month for the Landsat TOA scenes (1984 to 2015) covering the Tempisque watershed (tile path = 16, tile row = 53). The central line is the median, and box edges are the 25th (q_1) and 75th (q_3) percentiles. Points are shown as outliers if $> q_3 + 1.5(q_3 - q_1)$ or $< q_1 - 1.5(q_3 - q_1)$. The horizontal dotted line indicates the threshold above which images are excluded from further analysis. (b) Number of images per month for LAN.TOA and LAN.G-8dNDVI datasets (1984 to 2015) showing lower numbers of images during the rainy season (May through October). This is exacerbated when images with cloud cover greater than 25% are excluded (LAN.TOA 25).

Comparison and Evaluation of Image Collections

NDVI values were compared across datasets (fig. 7). LAN.G-8dNDVI remained a persistent outlier (figs. 7a, 7b, 7c, and 7g). Because it did not include metadata on cloud cover for straightforward filtering, we excluded that data collection from further analysis. The higher NDVI values resulting from application of the GEE *Landsat.simpleCloudScore* algorithm on the LAN.TOA collection (figs. 7d and 7e) suggested that it successfully identified pixels contaminated by clouds and should be used to exclude those pixels during aggregation. This was also confirmed by visual inspection of images before and after cloud masking. However, because cloud shadow is not detected by this function, images with global cloud cover greater than 25% were also excluded. Scene-wide screening is generally unfavorable, as it can exclude images with substantially useful pixels. However, until shadow detection masks, such as defined by the FMASK algorithm (Zhu and Woodcock, 2012), are available in GEE, this was the safest approach to avoid inclusion of cloud-contaminated pixels. The dataset-to-dataset comparisons suggest that Landsat TOA and LEDAPS provide similar results, with a linear relationship of slope close to 1 and intersect of 0.046 (fig. 7f). Because the more advanced LEDAPS processing algorithms are not available for Landsat 4 and 8, we favored the Landsat TOA collection (LAN.TOA 25 15) for further analysis. Both MODIS NDVI collections showed similar results (fig. 7i). Therefore, we chose the images provided by USGS-LPDAAC (MOD.U-16dNDVI) because of their finer spatial resolution. Finally,

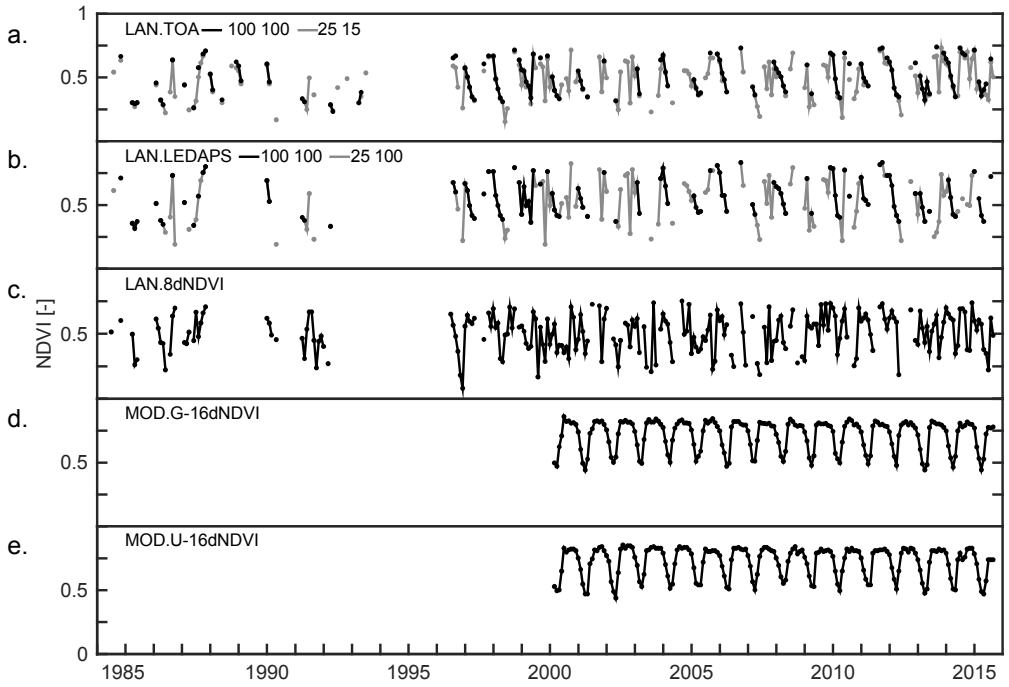

Figure 6. Time series of NDVI monthly maximum median values. Median was calculated over the entire Tempisque watershed: (a) Landsat TOA considering all scenes and pixels (gray lines) and excluding scenes with >25% cloud cover and pixels with >15% cloud cover (black lines), (b) Landsat LEDAPS, (c) Landsat 8-day NDVI, (d) MODIS 16-day NDVI by Google, and (e) MODIS 16-day NDVI by USGS-LPDAAC.

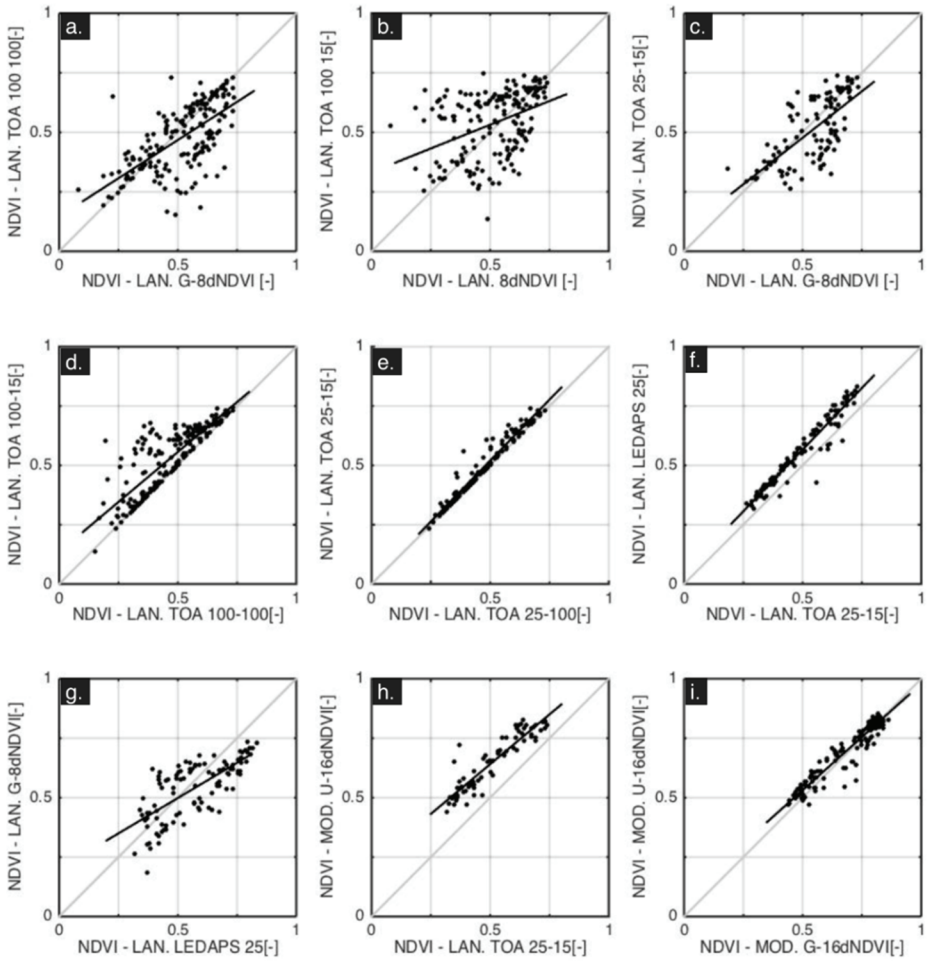

Figure 7. Comparison of the NDVI monthly maximum median values generated from one set of satellite imagery as compared to another. Median was calculated over the entire Tempisque watershed. For the LAN.TOA and LAN.LEDAPS collections, the numbers on the axis labels indicate the percentage of cloud cover above which images (first number) and pixels (second number, only applies to LAN.TOA) have been excluded.

NDVI time series were generally in agreement across the Landsat TOA, LEDAPS, and MODIS datasets. The slope of the relationship was generally close to 1, but always with a bias. Therefore, the general pattern of NDVI across datasets is comparable, but the absolute NDVI values are not. In summary, the choice between the Landsat and MODIS collections depends on the particular application. There is a trade-off between the temporal resolution of existing and reliable data, the time range covered, and the spatial resolution. Because of the higher temporal occurrence of coverage by MODIS, and hence the higher probability of capturing cloud-free data, use of the MODIS collection should be prioritized for such a tropical region, particularly if the coarser spatial resolution and shorter time coverage are not a limitation.

Implications for Tempisque Case Study

Landsat maps of NDVI in March 1986 and March 2011 suggest that the entire watershed witnessed an overall increase in vegetation greenness and hence cover (fig. 8a). This change is explained by the abandonment of cattle ranging in the region since the 1980s and natural succession to secondary forest. An increase in vegetation greenness also occurred in the PVNP, where dark areas in 1986 correspond to open water, most of which were entirely green in 2011. This change matches the known cattail invasion of the waterway, resulting in degradation of the wetland as a site for migratory birds and other endangered species. However, these two single pictures have to be considered cautiously considering the high inter-annual variability of vegetation dynamics caused by variations in precipitation and other drivers, and the artifact possibly caused by distinct image acquisition sources (Landsat 5 and Landsat 7). Within-season variability in greenness can be tracked using the MOD.U-16dNDVI dataset (fig. 8b). The contrast in greenness between March 2014 and July 2014 shows that MODIS images can provide sufficient detail despite their coarser spatial resolution. NDVI maps were selected for illustration, but NDVI maps for any other date can be promptly generated with GEE.

NDVI time series for the eleven polygons within the Tempisque watershed (fig. 2) were generated from the selected Landsat and MODIS collections (fig. 9). The time series from MODIS do not have any missing values but only extend back to the year 2000. A strong seasonal pattern is visible for all eleven polygons (fig. 9), suggesting that vegetation is mainly driven by precipitation. Missing data early and within the time series limit the use of Landsat for studies on temporal dynamics at monthly resolution. However, the relationship established between NDVI from MOD.U-16dNDVI and LAN.TOA (fig. 7h) can be used to fill in missing values. Future research will include use of the resulting signal to hindcast NDVI values prior to 2000 with techniques that capture the underlying pattern and cyclical components, e.g., singular spectral analysis with CatMV software (Golyandina and Osipov, 2006) conditioned by the scattered but existing Landsat values (fig. 9). Despite their limitation in generating time series of higher temporal resolution for this region of the globe, the Landsat images remain a valuable source for vegetation mapping and observation of changes and trends in land cover and land use through time. GEE provides a comprehensive suite of tools to undertake such analysis. However, other drivers might have caused inter-annual and intra-annual variations. We will continue to explore other hydrological and socio-economic drivers that might have caused these inter-annual and intra-annual variations in vegetation (fig. 1).

Conclusions, Limitations, and Opportunities

The mechanisms governing complex coupled human and natural systems may be unraveled with a comprehensive set of long-term time series of response and hypothesized explanatory covariates, including ecological, hydrological, and

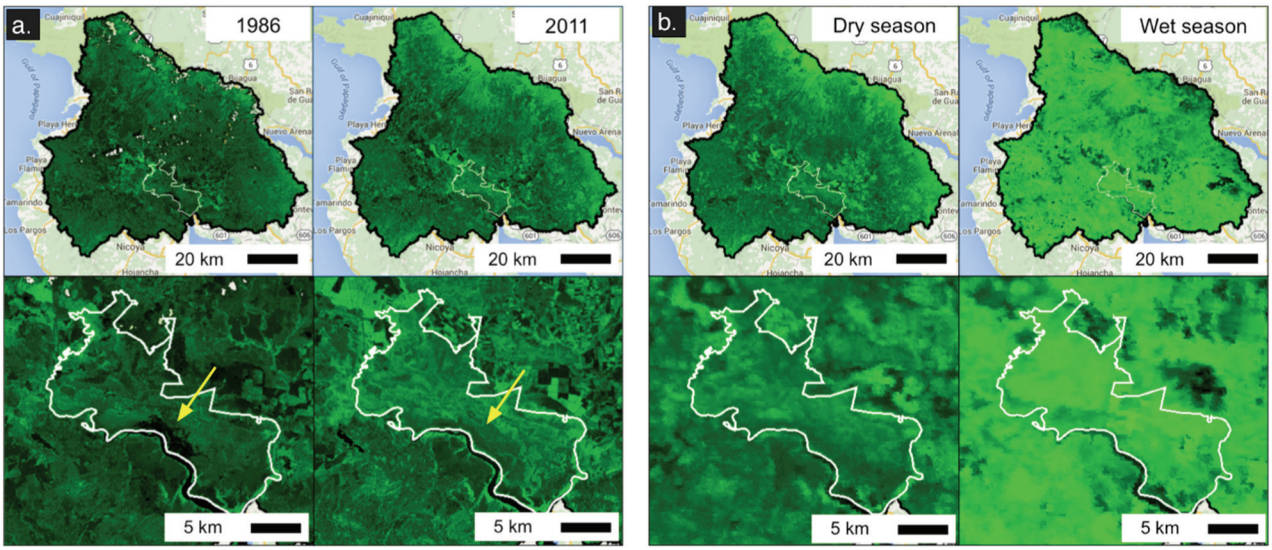

Figure 8. NDVI values for Tempisque (top) and zoom on Palo Verde National Park (bottom): (a) from LAN.TOA 25 15 collection in March 1986 (Landsat 5) and March 2011 (Landsat 7), and (b) from MOD.U-16dNDVI during dry (March 2014) and wet (October 2014) seasons. Color scale ranges from black (NDVI <= 0) to bright green (NDVI = 1).

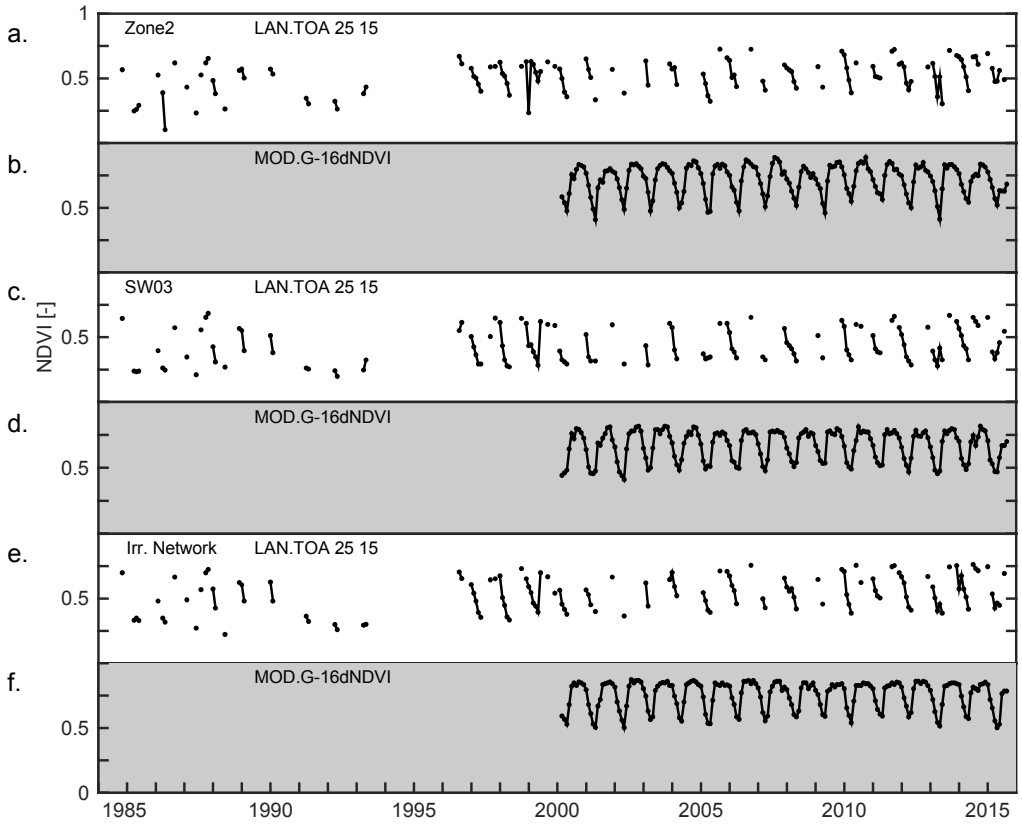

Figure 9. Time series of NDVI monthly maximum median values over a subset of three polygons (fig. 2). Median calculated over the entire Tempisque watershed. White background color: from Landsat-TOA excluding scenes with >25% cloud cover and pixels with >15% cloud cover at the pixel scale (LAN.TOA 25 15).

socio-economic drivers. In many situations, the vegetation covariate has not been measured with sufficient spatio-temporal resolution. This is especially the case for large-area ecosystems and wetland systems that are difficult to access for monitoring. With more than four decades of data, satellites provide a compelling alternative for generation of historical datasets of land cover and vegetation at different spatio-temporal scales. Until recently, access to this mine of information was limited to the remote sensing community, with substantial resources required to conduct such analysis. Open datasets (initially the MODIS data, and eventually the Landsat archive) catalyzed changes in processing algorithm strategies, and the recent creation of the Google Earth Engine (GEE) has provided a tool for other end users to enact these new strategies. In this article, we showed that the GEE platform provides an opportunity for engineers and scientists with limited knowledge of remote sensing to readily manipulate and extract information from remotely sensed data and create customized time series datasets and maps.

We illustrated this potential with a case study of the severely degraded Palo Verde National Park wetland, located within the Tempisque watershed in Costa Rica. We used GEE to map the temporal evolution of NDVI and generate spatially aggregated NDVI time series over eleven polygons dividing the study area. The resulting time series encode patterns in both spatial and temporal vegetation dynamics. The case study also demonstrated how GEE facilitates detection of cloud-contaminated images and pixels, and simplifies comparison of the many imagery sources available for vegetation mapping in a common spatial framework and computing environment. The resulting vegetation time series will be tested against time series of covariates, such as human activities and natural processes in the Tempisque watershed, to draw inferences about the causal effects underlying the vegetation dynamics.

For the sake of simplicity in this study, we considered NDVI as sufficient to capture the general vegetation dynamics, although its use for wetland systems can be limited by interference from high soil moisture. However, the general time series generation procedure described here can be applied for other indicators that can be generated within GEE.

This analysis would not have been feasible with the limited resources available without GEE. Based on prior experience in other systems, we estimate that the effort and cost involved in processing remote sensing data (e.g., acquiring imagery, software, and computing resources; image colocation, cloud screening, and filtering; time-series analysis) are at least an order of magnitude lower than with traditional approaches. Moreover, the GEE platform allowed easy comparison across processing platforms within a sensor family, and across different sensor types. By lowering the costs of historical image analysis, the GEE platform promises to catalyze scientific exploration of satellite archives across many disciplines.

SUPPLEMENTARY MATERIAL

Videos of the satellites scenes and the commented GEE script used in this study are hosted at https://figshare.com/s/

ed1a61c843bf8c98e383. For GEE users, the URL link to our commented GEE script is https://code.earthengine.google.com/60522444844bcb4833de530bf422db38.

ACKNOWLEDGEMENTS

The authors thank the Google Earth Engine team for the support provided through their forum and during the 2015 Google Earth Engine Summit. We also thank the University of Florida Department of Agricultural and Biological Engineering and Institute of Food and Agricultural Sciences (IFAS) for financial support. The corresponding author acknowledges support from the University of Florida Water Institute Faculty Fellowship. This work was financed in part by NSF Project No. CNIC OISE-1132840.

REFERENCES

Adam, E., Mutanga, O., & Rugege, D. (2010). Multispectral and hyperspectral remote sensing for identification and mapping of wetland vegetation: A review. *Wetlands Ecol. Mgmt., 18*(3), 281-296. http://dx.doi.org/10.1007/s11273-009-9169-z

Boyd, D. S., & Danson, F. M. (2005). Satellite remote sensing of forest resources: Three decades of research development. *Prog. Phys. Geog., 29*(1), 1-26. http://dx.doi.org/10.1191/0309133305pp432ra

Calvo-Alvarado, J., & Arias, O. R. (2005). Estudio de intercepción de lluvia de palo verde (*Parkinsonia aculeata*) en el Parque Nacional Palo Verde, Guanacaste, Costa Rica. Cartago, Costa Rica: Instituto Tecnológico de Costa Rica. San José, Costa Rica: Organization for Tropical Studies.

Calvo-Alvarado, J., & Arias, O. R. (2006). Estudio de evapotraspiración de la tifa (*Typha domingensis*) en el Parque Nacional Palo Verde, Guanacaste, Costa Rica. Cartago, Costa Rica: Instituto Tecnológico de Costa Rica. San José, Costa Rica: Organization for Tropical Studies.

Campo-Bescós, M. A., Muñoz-Carpena, R., Kaplan, D. A., Southworth, J., Zhu, L., & Waylen, P. R. (2013). Beyond precipitation: Physiographic gradients dictate the relative importance of environmental drivers on savanna vegetation. *PLoS One, 8*(8), e72348. http://dx.doi.org/10.1371/journal.pone.0072348.s005

Castillo-Núñez, M., & Guzmán Álvarez, J. A. (2004). Cambios en cobertura vegetal en Palo Verde según SIG. *Ambientico, 129*, 4-6.

Chen, L., Jin, Z., Michishita, R., Cai, J., Yue, T., Chen, B., & Xu, B. (2014). Dynamic monitoring of wetland cover changes using time-series remote sensing imagery. *Ecol. Informatics, 24*, 17-26. http://dx.doi.org/10.1016/j.ecoinf.2014.06.007

Christensen, E. J., Jensen, J. R., Ramsey, E. W., & Mackey, H. E. (1988). Aircraft MSS data registration and vegetation classification for wetland change detection. *Intl. J. Remote Sens., 9*(1), 23-38. http://dx.doi.org/10.1080/01431168808954834

Cohen, W. B., & Goward, S. N. (2004). Landsat's role in ecological applications of remote sensing. *BioScience, 54*(6), 535-545. http://dx.doi.org/10.1641/0006-3568(2004)054[0535:lrieao]2.0.co;2

Convertino, M., Muñoz-Carpena, R., & Murcia, C. (2016). "Reading the minds" for quantitative sustainability: Assessing stakeholder mental models via probabilistic text analysis. In J. Zhang, L. F. Luna-Reyes, T. A. Pardo, & D. S. Sayogo (Eds.), *Information, models, and sustainability: Policy informatics in the age of big data and open government* (pp. 21-38). Cham, Switzerland: Springer International.

Daniels, A. E. (2004). Protected area management in the watershed context: A case study of Palo Verde National Park, Costa Rica. MS thesis. Gainesville, FL: University of Florida.

Daniels, A. E., & Cumming, G. S. (2008). Conversion or conservation? Understanding wetland change in northwest Costa Rica. *Ecol. Appl., 18*(1), 49-63. http://dx.doi.org/10.1890/06-1658.1

Dennison, W. C., Orth, R. J., Moore, K. A., Stevenson, J. C., Carter, V., Kollar, S., ... Batiuk, R. A. (1993). Assessing water quality with submersed aquatic vegetation. *BioScience, 43*(2), 86-94. http://dx.doi.org/10.2307/1311969

Detto, M., Molini, A., Katul, G., Stoy, P., Palmroth, S., & Baldocchi, D. (2012). Causality and persistence in ecological systems: A nonparametric spectral Granger causality approach. *American Naturalist, 179*(4), 524-535. http://dx.doi.org/10.1086/664628

Finlayson, C. M., & Spiers, A. G. (1999). Global review of wetland resources and priorities for wetland inventory. Supervising Scientist Report 144. Wetlands International Publication 53. Canberra, Australia: Environment Australia, Supervising Scientist. Retrieved from https://www.environment.gov.au/system/files/resources/b7be7f68-4522-4aa5-8e86-de5cabd21645/files/ssr144-full-report-web.pdf

Golyandina, N., & Osipov, E. (2006). Caterpillar-SSA: Time series analysis and forecasting. St. Petersburg, Russia: St. Petersburg University, Department of Mathematics, GistaT Group. Retrieved from http://www.gistatgroup.com/cat/index.html.

Google. (2015). Google Earth Engine: A planetary-scale geospatial analysis platform. Mountain View, Cal.: Google Inc. Retrieved from https://earthengine.google.com

Gottschalk, T. K., Huettmann, F., & Ehlers, M. (2005). Review article: Thirty years of analysing and modelling avian habitat relationships using satellite imagery data: A review. *Intl. J. Remote Sens., 26*(12), 2631-2656. http://dx.doi.org/10.1080/01431160512331338041

Hansen, M. C., Potapov, P. V., Moore, R., Hancher, M., Turubanova, S. A., Tyukavina, A., ... Townshend, J. R. (2013). High-resolution global maps of 21st-century forest cover change. *Science, 342*(6160), 850-853. http://dx.doi.org/10.1126/science.1244693

Hassani, H. (2007). Singular spectrum analysis: Methodology and comparison. *J. Data Sci., 5*, 239-257.

Hornberger, G. M., & Spear, R. C. (1981). An approach to the preliminary analysis of environmental systems. *J. Environ. Mgmt., 12*(1), 7-18.

Houhoulis, P. F., & Michener, W. K. (2000). Detecting wetland change: A rule-based approach using NWI and SPOT-XS data. *Photogram. Eng. Remote Sens., 66*(2), 205-211.

Huffaker, R., & Canavari, M. (2015). A nonlinear dynamics approach to evaluating the "realism" of food systems models. Rome, Italy: United Nations FAO. Retrieved from http://www.fao.org/fileadmin/templates/ags/docs/MUFN/CALL_FILES_EXPERT_2015/CFP3-05_Full_Paper.pdf

Jensen, J. R., Ramsey, E. W., Christensen, E. J., & Sharitz, R. P. (1987). Inland wetland change detection using aircraft MSS data. *Photogram. Eng. Remote Sens., 53*(521-529).

Jiménez, J., González, E., & Mateo-Vega, J. (2001). Perspectives for the integrated management of the Tempisque River basin, Costa Rica. San José, Costa Rica: Organization for Tropical Studies.

Justice, C., & Townshend, J. (2002). Special issue on the moderate resolution imaging spectroradiometer (MODIS): A new generation of land surface monitoring. *Remote Sens. Environ., 83*(1-2), 1-2. http://dx.doi.org/10.1016/S0034-4257(02)00083-4

Kennedy, R. E., Andréfouët, S., Cohen, W. B., Gómez, C., Griffiths, P., Hais, M., ... Zhu, Z. (2014). Bringing an ecological

view of change to Landsat-based remote sensing. *Front. Ecol. Environ., 12*(6), 339-346. http://dx.doi.org/10.1890/130066
Kennedy, R. E., Townsend, P. A., Gross, J. E., Cohen, W. B., Bolstad, P., Wang, Y. Q., & Adams, P. (2009). Remote sensing change detection tools for natural resource managers: Understanding concepts and tradeoffs in the design of landscape monitoring projects. *Remote Sens. Environ., 113*(7), 1382-1396. http://dx.doi.org/10.1016/j.rse.2008.07.018
Kushwaha, S. P. S., Dwivedi, R. S., & Rao, B. R. M. (2000). Evaluation of various digital image processing techniques for detection of coastal wetlands using ERS-1 SAR data. *Intl. J. Remote Sens., 21*(3), 565-579. http://dx.doi.org/10.1080/014311600210759
Larsen, L., Thomas, C., Eppinga, M., & Coulthard, T. (2014). Exploratory modeling: Extracting causality in complex systems. *EOS, 95*(32), 285-292.
Lu, D., Mausel, P., Brondizio, E., & Moran, E. (2004). Change detection techniques. *Intl. J. Remote Sens., 25*(12), 2365-2401. http://dx.doi.org/10.1080/0143116031000139863
Masek, J. G., Vermote, E. F., Saleous, N. E., Wolfe, R., Hall, F. G., Huemmrich, K. F., ... Lim, T.-K. (2006). A Landsat surface reflectance dataset for North America, 1990-2000. *IEEE Geosci. Remote Sens. Lett., 3*(1), 68-72. http://dx.doi.org/10.1109/LGRS.2005.857030
McCoy, M. B., & Rodríguez, J. M. (1994). Cattail (*Typha domingensis*) eradication methods in the restoration of a tropical, seasonal, freshwater marsh. In W. J. Mitsch (Ed.), *Global wetlands: Old world and new* (pp. 469-482). Amsterdam, The Netherlands, Elsevier Science.
Mitsch, W. J., & Gosselink, J. G. (2000). The value of wetlands: Importance of scale and landscape setting. *Ecol. Econ., 35*(1), 25-33. http://dx.doi.org/10.1016/S0921-8009(00)00165-8
Mitsch, W. J., & Gosselink, J. G. (2007). *Wetlands.* Hoboken, NJ: John Wiley & Sons.
Moreno-Mateos, D., Power, M. E., Comin, F. A., & Yockteng, R. (2012). Structural and functional loss in restored wetland ecosystems. *PLoS Biol., 10*(1), e1001247. http://dx.doi.org/10.1371/journal.pbio.1001247
Munyati, C. (2000). Wetland change detection on the Kafue Flats, Zambia, by classification of a multitemporal remote sensing image dataset. *Intl. J. Remote Sens., 21*(9), 1787-1806. http://dx.doi.org/10.1080/014311600209742
Osland, M. J., Gonzalez, E., & Richardson, C. J. (2011). Restoring diversity after cattail expansion: Disturbance, resilience, and seasonality in a tropical dry wetland. *Ecol. Appl., 21*(3), 715-728. http://dx.doi.org/10.1890/09-0981.1
Ottino, J. M. (2004). Engineering complex systems. *Nature, 427*(6973), 399-399. http://dx.doi.org/10.1038/427399a
Pittman, K., Hansen, M. C., Becker-Reshef, I., Potapov, P. V., & Justice, C. O. (2010). Estimating global cropland extent with multi-year MODIS data. *Remote Sens., 2*(7), 1844. http://dx.doi.org/10.3390/rs2071844
Ramsey, E. W., & Laine, S. C. (1997). Comparison of Landsat thematic mapper and high-resolution photography to identify change in complex coastal wetlands. *J. Coastal Res., 13*(2), 281-292. Retrieved from http://www.jstor.org/stable/4298625
Schreiber, T. (1999). Interdisciplinary application of nonlinear time series methods. *Physics Reports, 308*(1), 1-64.
Sugihara, G., May, R., Ye, H., Hsieh, C.-H., Deyle, E., Fogarty, M., & Munch, S. (2012). Detecting causality in complex ecosystems. *Science, 338*(6106), 496-500. http://dx.doi.org/10.1126/science.1227079
Trama, F. A., Rizo-Patrón, F. L., Kumar, A., González, E., Somma, D., & McCoy C., M. B. (2009). Wetland cover types and plant community changes in response to cattail-control activities in the Palo Verde Marsh, Costa Rica. *Ecol. Restor., 27*(3), 278-289. http://dx.doi.org/10.3368/er.27.3.278
Tucker, C., Pinzon, J., Brown, M., Slayback, D., Pak, E., Mahoney, R., Vermote, E., & El Saleus, N. (2005). An extended AVHRR 8-km NDVI dataset compatible with MODIS and SPOT vegetation NDVI data. *Intl. J. Remote Sensing, 26*(20), 4485-4498. http://doi.org/10.1080/01431160500168686
van Dam, R. A., Camilleri, C., & Finlayson, C. M. (1998). The potential of rapid assessment techniques as early warning indicators of wetland degradation: A review. *Environ. Toxicol. Water Qual., 13*(4), 297-312. http://dx.doi.org/10.1002/(SICI)1098-2256(1998)13:4<297::AID-TOX3>3.0.CO;2-2
Vaughan, C., McCoy, M., Fallas, J., Chaves, H., Barboza, G., Wong, G., & Carbonell, M. (1996). Plan de manejo y desarrollo del Parque Nacional Palo Verde y Reserva Biologica Lomas Barbudal. Contrato SENARA-BID-MINAE-UNA.
Wulder, M. A., & Masek, J. G. (2012). Preface to Landsat legacy special issue: Continuing the Landsat legacy. *Remote Sens. Environ., 122*, 1. http://dx.doi.org/10.1016/j.rse.2012.01.009
Xie, Y., Sha, Z., & Yu, M. (2008). Remote sensing imagery in vegetation mapping: A review. *J. Plant Ecol., 1*(1), 9-23. http://dx.doi.org/10.1093/jpe/rtm005
Zhao, B., Yan, Y., Guo, H., He, M., Gu, Y., & Li, B. (2009). Monitoring rapid vegetation succession in estuarine wetland using time series MODIS-based indicators: An application in the Yangtze River Delta area. *Ecol. Indic., 9*(2), 346-356. http://dx.doi.org/10.1016/j.ecolind.2008.05.009
Zhu, Z., & Woodcock, C. E. (2012). Object-based cloud and cloud shadow detection in Landsat imagery. *Remote Sens. Environ., 118*, 83-94. http://dx.doi.org/10.1016/j.rse.2011.10.028
Zuñiga, E. (1993). Districto de Riego Arenal Zapandi. *Agronomia Costarricense, 17*(2), 87-94.

View publication stats